Advanced Healthcare Materials

ADVANCED HEALTHCARE MATERIALS
www.advhealthmat.de

RESEARCH ARTICLE OPEN ACCESS

Highly Tunable and Cell-Remodelable Thiol-ene Alginate-Peptide Crosslinked Hydrogels to Recreate Cellular and Organoid Microenvironments for Biofabrication

Julia Fernández-Pérez | Adrián Seijas-Gamardo | Antonio J. Feliciano | Panagiota Kakni | Anna M. Kip | Paul Wieringa | Stefan Giselbrecht | Matthew B. Baker | Lorenzo Moroni

MERLN Institute for Technology-Inspired Regenerative Medicine, Maastricht University, Maastricht, The Netherlands

Correspondence: Julia Fernández-Pérez (julia.fernandez.perez@tuwien.ac.at) | Matthew B. Baker (m.baker@maastrichtuniversity.nl) | Lorenzo Moroni (l.moroni@maastrichtuniversity.nl)

Received: 1 September 2025 | **Revised:** 14 November 2025 | **Accepted:** 22 November 2025

Keywords: alginate | cellular microenvironment | hydrogels | organoids | thiol-ene chemistry

ABSTRACT

In this study, a cell-mediated degradable alginate hydrogel system for organoid culture and amenable to biofabrication technologies is presented. Norbornene-functionalized alginate is crosslinked with a di-thiolated peptide sequence cleavable by matrix metalloproteinases and decorated with cysteine-terminated cell-adhesion peptide RGD, upon exposure to UV. Stiffness of the hydrogels can be controlled by tuning polymer and crosslinker concentrations. Pre-gel solutions are successfully bioprinted with a pneumatic extrusion-based system. The hydrogels are used to encapsulate a variety of sensitive cell types. Human endometrial organoids present high cell viability, grow in size over time, present spherical morphology, and express cell–cell contacts E-cadherin and proliferation marker Ki67. Encapsulated mouse embryonic stem cell-derived thyroid follicles produce thyroglobulin and T4. Mouse intestinal organoids adopt a proliferative phenotype. Vascularization inside the hydrogels is achieved using endothelial cells and supporting cells (single cell suspension and spheroids). Neurite outgrowth, both small and thick bundles, from encapsulated iPSC-derived neurospheres, demonstrates the reinnervation potential of the hydrogel. This polysaccharide hydrogel platform could be used as a defined, tunable, and ethical alternative to mouse sarcoma-extracted basement-membrane matrices.

1 | Introduction

Organoids and 3D organotypic tissue models have revolutionized the biomedical research field, improving our understanding of organs in their healthy as well as diseased states [1]. Improvements in biofabrication techniques are allowing to increase the complexity of these models [2, 3]. Applications in screening of drugs and therapies make these models highly attractive because of their higher biomimicry of native tissues and better sensitivity compared to conventional 2D and 3D tissue models. Compared to spheroids or organoids developed in low-adhesion surfaces, encapsulation in 3D matrices also fosters cell-matrix interactions, mimicking the native microenvironment [4]. It has recently been shown that kidney organoids encapsulated in supramolecular fibrous hydrogels shift differentiation toward glomerular lineages, compared to the free-floating organoids, even with the same medium composition [5]. Furthermore, epithelial-stromal cross-talk can be recapitulated by encapsulation, for example in endometrial models [6], or models of trophoblast invasion [7]. Such results would not have been possible in 2D cultures. 3D cell culture has traditionally been very dependent on the use of Matrigel, a basement-membrane matrix extracted from

Engelbreth–Holm–Swarm mouse sarcomas. It is mainly composed of laminin, collagen IV, entactin and perlecan, as well as ill-defined amounts of growth factors, transcription factors and cytokines [8, 9]. Its main limitations are the wide variability in composition and presence of xenogenic contaminants, such as lactate dehydrogenase-elevating virus [10]. Other natural materials based on purified extracellular matrix (ECM) proteins (collagen type I, laminin, vitronectin or fibrinogen) also suffer from batch-to-batch variability and their biochemical properties cannot be decoupled from their mechanical properties [10].

To overcome the aforementioned caveats of using animal-isolated materials to produce hydrogels for 3D cell culture, great efforts have been placed in developing controllable synthetic materials as alternatives to Matrigel [10]. The goal is to use an inert polymer as a blank slate to simultaneously be able to tune key physical, mechanical and biological properties independently, by modifying parameters such as molecular weight, crosslinking density, polymerization method, or biofunctionalization. Among the most used polymers is polyethylene glycol (PEG) as it is hydrophilic, bioinert and highly amenable to chemical modification. PEG hydrogels for cell encapsulation have been made by many crosslinking chemistries including (but not limited to) light-reactive groups (acrylate [11] and thiol-ene [12]), Michael-addition (maleimide-thiol [13, 14] and vinyl-sulfone [15, 16]), or enzymatic reactions (transglutaminase enzyme factor XIIIa [17, 18]). While being considered bioinert, with low toxicity and generally recognized as safe (GRAS) by the FDA, concerns over PEG immunogenicity have been raised as a high prevalence of anti-PEG antibodies in the general public has been reported [19, 20]. This might be worsened today by the widespread use of PEG for the formulation of lipid nanoparticle mRNA vaccines against SARS-CoV-2 [21]. Further, PEG based hydrogels (or pre-hydrogels) generally have a tradeoff between processability (high wt%, high viscosity) or cell compatibility (low wt%, low viscosity) when it comes to biofabrication.

Alginate can also be used as a blank-slate polymer amenable to chemical modifications [22] such as oxidation (imine-type modifications) [23], methacrylation (free radical) [24], strain-promoted azide-alkyne cycloaddition (SPAAC) bio-orthogonal click-chemistry [25], Michael-additions (maleimide-thiol [26]), host-guest chemistry (cyclodextrin-adamantane) [27] and norbornene (thiol-ene) [28, 29]. Alginate is a bio-based polymer, but not animal-derived which avoids problems associated with xenogeneic materials. Alginate is biocompatible, has low toxicity, is relatively low cost, and is widely used for 3D encapsulation [30]. Chemical modifications on alginate are typically pendant, in contrast to the telechelic nature of PEG modifications. This distinction allows alginate modifications to retain the polymer backbone's integrity and provides greater flexibility in tuning its physical and biological properties without affecting its structural framework. Other natural polysaccharides that have been modified to be crosslinked via thiol-ene chemistries are citrus pectin [31] and fungal pullulan [32], but alginate remains more widely used. As many biopolymers, the main challenges with alginates are the sourcing, purification, and batch-to-batch variability in starting materials.

We have previously shown the possibility of modifying alginate to contain norbornene groups for thiol-ene reactions in presence of a photoinitiatior and UV light [28]. Thiol-ene crosslinking has several advantages over other crosslinking mechanisms including high biocompatibility, fast kinetics, and low oxygen inhibition [33]. Proof-of-concept experiments using robust cell lines showed high cell viability upon encapsulation in alginate-norbornene hydrogels [28]. Furthermore, such hydrogels were used to encapsulate hiPSC-derived renal organoids. When organoids were encapsulated, fibrosis was reduced, compared to hydrogel-free (non-encapsulated) organoids [34]. These two approaches used 4-arm thiolated PEG as crosslinker and thus rendered these hydrogels non-degradable by cell activity. We have recently shown that by using a matrix metalloproteinase (MMP)-cleavable peptide sequence flanked by cysteines (thiol-containing aminoacid) as crosslinker, immortalized renal proximal tubule epithelial cells formed cystic aggregates which were not present in non-degradable formulations [35].

The aim of this work is to establish a material platform amenable to biofabrication technologies for the culture of organoids and organotypic tissue models based on cell-mediated degradable alginate hydrogels. We could tune mechanical properties, such as viscosity and stiffness, pre- and post-gel formation by modifying the polymer content and/or the crosslinker concentration. A wide variety of sensitive cell types were encapsulated in these hydrogels, presenting high cell viability, proliferation potential, and desired phenotype. The potential for vascularization and innervation of organoids was evaluated.

2 | Materials and Methods

2.1 | Purification of Alginate

Sodium alginate powder (FMC Manugel GMB, Lot No. G9402001, ≈380 kDa) was purified as follows. A 1% (w/v) solution in ultrapure water was prepared by overnight dissolution at 4°C under constant stirring. Activated charcoal (0.5% (w/w), Sigma) was added and stirred for a further 24 h at 4°C. Solution was centrifuged to precipitate the largest charcoal particles. The solution was passed then through a series of filters, 11, 1.2, 0.45, and 0.2 µm, under vacuum. The solution was passed through each filter until the membrane was no longer clogged before passing it through the next smaller pore filter. Solutions were stored at 4°C in between days, as this process took 3 days. Finally, the purified alginate solution was frozen and lyophilized. A white fibrous powder was obtained (yield: 6–7 g). Material was stored in a closed tight container at -20°C.

2.2 | Coupling of Norbornene Functional Groups to Alginate by DMTMM

Coupling of norbornene to alginate was performed following our previously reported method [29]. Briefly, 1 g of purified alginate (5.05×10^{-3} mol COOH groups) was dissolved in 100 mL of MES buffer (pH adjusted to 6.5 with NaOH) in a glass vial. Then, 4-(4,6-Dimethoxy-1,3,5-triazin-2-yl)-4-methylmorpholinium chloride (DMTMM, Sigma) (1.4 g, 5.05×10^{-3} mol 1:1 equiv. to alginate COOH groups) was added to the alginate solution until dissolved. Then, 5-Norbornene2-methylamine (0.195 mL, 1.52×10^{-3} mol, 0.3 equiv., TCI

chemicals) was added. The reaction was left to stir for 24 h at room temperature. The solution was then transferred to a 10 kDa MWCO dialysis tube (SnakeSkin, ThermoFisher) and dialyzed against decreasing NaCl concentrations. Each solution was changed after 10 – 18 h, starting from 100 mM NaCl, then 50 mM NaCl, 25 mM, and finally distilled water. The alginate-norbornene product was then frozen and lyophilized, yielding a white fibrous solid. Material was stored in a closed tight container at -20°C. The work presented here was all done with one batch to ensure functionalization was consistent throughout.

Degree of functionalization was determined by 1H NMR (700 MHz Bruker spectrometer at 325 °K with water suppression applied). Between 4 and 5 mg of alginate-norbornene were dissolved in 0.6 mL of D2O with 2 mM DMF standard. By integrating the norbornene double bonds ($\delta = 5.9{-}6.3$ ppm, 2 H) relative to 2 mM nondeuterated DMF standard ($\delta = 8.02$ ppm, 1 H) in D2O, the percentage of functionalization was determined to be 7,1%. This resulted in 3.33×10^{-7} mol norbornene groups in every 1 mg of alginate-norbornene.

2.3 | General Gel Preparation

Alginate-norbornene solutions were prepared in PBS or unsupplemented medium (without serum or other additives), usually at double the final concentration needed (% w/v). CGGGRGDS (RGD, ChinaPeptides, China) was dissolved in PBS at 50 mM; crosslinkers, either an MMP-cleavable (referred to as degradable) sequence CGDGVPLSLYSGGDGC (Genscript, The Netherlands) or non-degradable PEG dithiol (Creative PEGWorks, MW 2k), were dissolved in PBS at 100 mM. Appropriate volumes of each component were added to the pre-gel solution. When cells needed to be included, they were added at this point, after harvesting according to the cell type's needs. Last, 200 mM stock Lithium phenyl-2,4,6-trimethylbenzoylphosphinate (LAP, Sigma) in PBS was added to a final concentration of 2 mM. The pre-gel solution was gently mixed using piston pipettes to ensure a homogeneous solution. 10 – 20 µL solution was deposited in between siliconized microscopy slides (Sigmacote, Sigma) separated with an O-ring, placed inside a 100 cm diameter open Petri dish and irradiated for 30 s with UV 365 nm at a distance of 10 cm, from a BioX bioprinter (Cellink). The laminar flow was turned on when cell-laden gels were prepared. Crosslinked gels were transferred immediately to culturing plates in a humidified incubator at 37°C or used for other characterization methods. Peptides, PEG, and LAP were dissolved just prior to use to prevent potential degradation or disulfide bridge formation. GFOGER and YIGSR peptides were also purchased from ChinaPeptides, and used at a final concentration of 2.5 mM.

2.4 | Rheology

Rheological measurements were performed using a DHR-2 rheometer from TA instruments equipped with a Peltier heating element, a 20 mm cone-plate geometry (a truncation of 2.002 with gap = 53 µm), a UV attachment (TA UV accessory) and 365 nm light source (Thor Labs). All measurements were performed at 25°C. Immediately after mixing, the pre-gel solutions (alginate-norbornene, MMP degradable crosslinker, RGD and LAP) were loaded on the rheometer, the cone and plate lowered to the geometry gap. Time sweep measurements were performed at a frequency of 2 rad/s, 2% strain, and measuring during 2 min, followed by 30 s of irradiation and another 2.5 min (total time 5 min).

2.5 | Swelling Test

Hydrogels used for swelling tests had a formulation of 3% w/v alginate-norbornene and 2 mM crosslinker (either MMP peptide or PEG). Gels of 20 µL were prepared as previously described without the addition of cells. Disk-shaped gels were weighed after crosslinking and then placed in 1 mL PBS for 24 h in an oven at 37°C. They were then weighed swollen, carefully removing excess liquid at the edges of the gel. The swelling ratio is presented as:

$$SR\ (\%) = 100 * \frac{swollen\ weight}{initial\ unswollen\ weight}$$

2.6 | Degradability Test

Hydrogels used for degradation tests had a formulation of 3% w/v alginate-norbornene and 2 mM crosslinker (either MMP peptide or PEG). Degradation tests were performed after swelling by incubation in 2 U/ml (2.4 µg/mL) collagenase I (Sigma) in PBS containing 0.36 mM $CaCl_2$ during 8 h at 37°C, weighing before and after. For fast visualization, hydrogels were incubated in 10 mg/ml collagenase for 1 h at 37°C, and pictures taken.

2.7 | Ultrastructure Analysis

Hydrogels used for SEM imaging had a formulation of 3% w/v alginate-norbornene and 2 mM MMP peptide crosslinker. Hydrogels were fabricated as described previously and allowed to swell overnight in distilled water. Samples were then snap frozen in liquid nitrogen and "hit" to produce cracks while frozen. Immediately thereafter, samples were placed in a freeze-dryer for a minimum of 3 h. After lyophilization, samples were sputter coated and imaged using a scanning electron microscope (Jeol JSM-IT200 InTouchScope, Japan).

2.8 | Printing

An acellular pre-gel solution (4% w/v alginate-norbornene, crosslinker and photoinitiator) was loaded in a 3 mL syringe and placed in the pneumatic extrusion cartridge of a commercial 3D bioprinter (BioX, Cellink). A metallic 22 G needle (inner diameter 0.41 mm) was secured to the syringe via luer lock. The printing parameters were fixed at a pressure of 50 kPa and a printing speed of 3 mm/s. Macroscopic pictures were taken and filament thickness measured in order to calculate the spreading ratio, according to the following formula.

$$Spreading\ ratio = \frac{measured\ thickness}{internal\ diameter\ nozzle}$$

2.9 | Encapsulation of Human Endometrial Organoids

Human endometrial organoids were harvested for passaging as follows, based on published protocols [36, 37]. Endometrial organoids were retrieved from Geltrex (Fisher Scientific, A1413302) domes by adding cold Cell Recovery Solution (Corning, 354253) and incubating the plate for 20 min on ice. Then, the domes were further disrupted mechanically by manual pipetting. Collected organoids were then centrifuged for 200 × *g* for 5 min. Supernatant was removed, 1 mL DMEM/F12 + 1% BSA added, and organoids were mechanically disrupted by passing the solution 5 to 6 times through a 22 G needle. Harvested organoids were centrifuged again for 200 × *g* for 5 min. The organoid fragments were resuspended in organoid media with 10 μM of Y-27632 (ROCK inhibitor) (STEMCELL Technologies, 72302). The adequate volume, never more than 5 μL, from the resuspension solution was added to the 20 μL pre-gel solution to obtain around 10 viable organoids per gel. The final gels were obtained after 30″ UV exposure (10 mW/cm^2). The hydrogels had a final composition of 1% w/v alginate-norbornene, 0.5 mM MMP-degradable crosslinker and 2.5 mM RGD. This formulation resulted in hydrogels that were very soft and challenging to handle, and thus not used for subsequent applications. Organoid-laden gels were immersed in 300 μL of medium containing 10 μM ROCK inhibitor. Medium was changed every second day, and ROCK inhibitor was only present for the first 2 days.

Viability was assessed after 7 days in culture by incubation of hydrogel-laden organoids in 1 μM Calcein-AM (Invitrogen), 2 μM Ethidium homodimer (Invitrogen) and 1 μg/ml Hoechst 33342 (Invitrogen) for 30 min in a humidified incubator at 37°C. After two brief washes with PBS, gels were ready for imaging.

In parallel, hydrogels were fixed after 7 days in culture in 4% paraformaldehyde at room temperature for 30 min. Immunocytochemistry was performed as follows. Samples were permeabilized for 30 min in 0.5% Triton-X100 (Sigma) in PBS and then blocked in 5% donkey serum for 1 h at room temperature. Then primary antibodies diluted in 0.5% donkey serum in PBS were added and incubated overnight at 4°C. Rabbit anti-Ki67 (ab15580, Abcam) and mouse anti-E-Cadherin (610181, Beckton Dickinson) were used at 1:500. After three 10-min washes in 0.5% goat serum in PBS a 2-h incubation with secondary antibodies 1:250 (goat anti-mouse conjugated to Alexa568, and donkey anti-goat conjugated to Alexa647), 0.25 μM Alexa488-conjugated phalloidin (Invitrogen) and 0,2 μg/mL DAPI (Sigma) was carried out. A further three 10-min washes in PBS were employed to remove any unbound dyes. Both the viability and immuno-cytochemistry stained gels were imaged with a Leica TCS SP8 STED laser scanning confocal microscope.

2.10 | Encapsulation of Mouse ESC-Derived Thyroid Follicles

Thyroid follicles were obtained from murine embryonic stem cells, according to Carvalho and colleagues [38], and Antonica and colleagues [39]. Briefly, mESCs were grown as embryoid bodies (EB) by hanging drop culture for 4 days. EBs were then embedded in Matrigel (GF-reduced) domes for 3 days with medium containing Doxycycline (1 μg/mL) and for further 14 days with 8-Br-cAMP (10×10^{-6} M). Differentiated follicles were harvested via incubation with collagenase type IV (17104019, Gibco, Waltham, USA) (100 U/ mL) and dispase II (04942078001, Roche, Basel, Switzerland) (4 U/mL). Large aggregates were removed by using a 100 μm cell strainer, and single cells or very small aggregates were let flow through a 30 μm strainer. Aggregates ranging from 30 μm to 100 μm were counted and concentration adjusted to encapsulate 100.000 follicles/mL gel. The final 20 μL gels consisted of 1% alginate-norbornene (w/v), 1 mM MMP and 2.5 mM RGD, including 2000 follicles. Follicles in the gels were cultured in differentiation medium supplemented with 8-Br-cAMP (10×10^{-6} M) and TGF-βRI inhibitor SB431542 (10×10^{-6} M, 1614, Tocris, Bristol, UK) for 4 days.

Cell-containing hydrogels were incubated with 1 μM Calcein–AM (Thermo) and 2 μM Ethidium homodimer (Thermo) in PBS for 1 h in a humidified incubator at 37°C. Hydrogels were washed once with PBS and immediately imaged in a microscope (Leica SP8).

Upon fixation, gels were blocked and permeabilized for 1 h at room temperature in a 3% BSA, 5% goat serum and 0.2% Triton X100 solution in HBSS. Primary antibodies rabbit anti-TG (1:700, A025102-2, Agilent) and mouse anti-T4 (1:100, MA5-14716, ThermoFisher), or Rabbit anti-Ki67 (1:500) (ab15580, Abcam) only, were incubated overnight at 4°C in blocking buffer. After 3 1-h washes in blocking buffer, samples were incubated with secondary antibody (1:500) for 3 h at room temperature.

2.11 | Encapsulation of Mouse Intestinal Organoids

Mouse embryonic intestinal organoids were harvested for passaging as described earlier by Kakni and colleagues [40]. Briefly, Matrigel domes containing organoids were treated with cold Gentle Cell Dissociation Reagent (STEMCELL Technologies), broken up pieces were collected and centrifuged at 290 × *g* for 5 min at 4°C. The supernatant was then removed, cold DMEM/F-12 with 15×10^{-3} M HEPES (STEMCELL Technologies) added, and further centrifuged at 200 × *g* for 5 min at 4°C. The pelleted organoids were then added to the pre-gel solution and 20 μL gels were obtained after 30″ UV exposure (as described above). The gel composition was 3% alginate-norbornene, 1 mM MMP crosslinker and 2.5 mM RGD. Organoid-laden gels were immersed in 650 μL of IntestiCult (STEMCELL Technologies), with media changes every 2 days. After 7 days of culture, samples were fixed in 4% PFA in PBS for 20 min at room temperature. Samples were blocked in 5% goat serum for 1 h at room temperature. Then primary antibodies diluted in 0.5% goat serum in PBS were added and incubated overnight at 4 °C. Rabbit anti-Ki67 (ab15580, Abcam) and mouse anti-E-Cadherin (610181, Beckton Dickinson) were used at 1:500. After 3 10-min washes in 0.5% goat serum in PBS, a 2-h incubation with secondary antibodies 1:500 (goat anti-mouse, and donkey anti-goat), 1:250 Alexa488-conjugated phalloidin (Invitrogen) and 1:250 DAPI (Sigma) was carried out. A further 3 × 10-min washes in PBS were employed to remove any unbound dyes. Gels were imaged in a confocal microscope (Leica SP8).

2.12 | Encapsulation of human Endothelial Cells

HUVECs were purchased from PromoCell, from pooled donors. Cells used in these experiments were used from cryopreserved vials and expanded before use at passages 4–6. The culture media used to expand these cells was EGM-2 bullet-kit (PromoCell).

Bone marrow-derived human mesenchymal stromal cells (MSCs) were purchased from Texas A&M Health Science Center, College of Medicine, Institute for Regenerative Medicine (Donor d8011L, female, age 22) and used at passage 5. Cells were expanded in alphaMEM (Gibco) supplemented with 10% FBS (Sigma). They were used as support cells for endothelial cells.

Two set-ups were employed to encapsulate the endothelial and support cells: as a single cell suspension and as pre-formed spheroids.

Single cells. Cells were trypsinized and counted. Endothelial cells and MSCs were mixed at a 9:1 ratio, at a final concentration of 6 $\times$ 10^6 endothelial cells and 0.6 $\times$ 10^6 MSC per mL gel (3% w/v alginate-norbornene, 1 mM MMP, 2.5 mM RGD). Medium was supplemented with 50 ng/mL VEGF-A (PeproTech). Viability was assessed after 7 days in culture by incubation in 1 μM Calcein-AM (Invitrogen), 2 μM Ethidium homodimer (Invitrogen) and 1 μg/mL Hoechst 33342 (Invitrogen) for 30 min in a humidified incubator at 37°C. After two brief washes with PBS, gels were ready for imaging. For each sample, confocal stacks were acquired at 2 different areas. Four images of each stack were quantified using ImageJ by splitting the channels of the live and dead signal, binarizing them and counting automatically using the analyze particles feature.

Spheroids. Endothelial cells and MSCs were mixed at a 9:1 ratio in cellulose (0,24% w/v) at a concentration of 25000 cells/mL. 40 μL droplets were formed on the lid of a 150 mm diameter Petri dish using a multichannel pipette. PBS was added on the bottom of the dish to reduce drying. Spheroids were allowed to form over 24 h in a humidified incubator (37°C, 5% CO_2, 21% O_2). Spheroids were then carefully collected with excess PBS to promote removal of methylcellulose, and pelleted by gentle centrifugation (5 mins, 100 $\times$ g). Spheroid concentration was adjusted to have 30 spheroids per 100 μL gel with a composition of 1% w/v alginate-norbornene, 1 mM MMP crosslinker and 2.5 mM RGD. Gels were cultured for 24 h and then processed for imaging as described below.

Hydrogels were washed once with PBS and then fixed in 4% PFA in PBS for 20 min at room temperature, followed by another wash with PBS. Blocking was performed for 2 h at room temperature in 5% goat serum and 0.5% Triton X100 in PBS. Primary antibodies were prepared in antibody buffer composed of 1% goat serum and 0.1% Triton X100 in PBS and incubated overnight. Mouse anti-CD31 (ab24590, Abcam) was used at 1:200. Three 1-h washing steps with antibody buffer were then performed. Secondary antibodies (Alexa488-conjugated goat anti-mouse, Thermo Fisher) were prepared in antibody buffer at 1:200 and incubated overnight. Then, a 30-min incubation with DAPI at 0.2 μg/mL in antibody buffer was performed followed by three 30-min washing steps with antibody buffer. All steps were performed at room temperature and on a rocking platform.

2.13 | Encapsulation of Human iPSC-Derived Neurospheres

Peripheral nervous system neurons were differentiated from human induced pluripotent stem cells (hiPSCs; LUMC0031iCTRL08) adapting an existing published protocol [41] to produce neurospheres. Shortly, 200 hiPSCs were seeded on 400 μm diameter agarose microwells in mTeSR Plus medium (STEMCELL Technologies, 100–1130) supplemented with 10 μM of ROCK inhibitor to form embryoid bodies. The next day ROCK inhibitor was removed and after 24 h the medium was supplemented with 1% of Dimethyl sulfoxide (DMSO), synchronizing cells for 48 h. Thereafter, the medium was changed to Advanced RPMI 1640 (Gibco) supplemented with 1% GlutaMAX, LDN-193189 hydrochloride and SB-431542. Cells were kept for 48 h in this medium. The medium was then supplemented with CHIR99021 and Retinoic acid and maintained for 4 days. Finally, the medium was supplemented with SU5402 and DAPT for 48 h, after which the neurospheres were ready to be seeded.

On the last day of the differentiation (14 days), the neurospheres were harvested from the agarose microwells, collected in a tube and waited for them to sediment by gravity. Supernatant was removed, neurospheres were resuspended in fresh medium and transferred into the pre-gel solution, to include 5–10 neurospheres per gel. 20 μL of pre-gel solution was casted in between Sigma-coted glass slides and UV irradiated 30″ (10 mW/cm^2). Gels had a composition of 1% alginate-norbornene, 1 mM MMP crosslinker and 2.5 mM RGD. Gels were then released and cultured in neural medium consisting of Neurobasal medium supplemented with N21 and 50 ng/mL of NGF for 8 days. Medium was changed every other day. The outgrowth of axons was recorded by brightfield imaging (and length quantified using ImageJ) and by confocal microscopy (Leica SP8) upon immunostaining of βIII tubulin. Upon fixation, gels were permeabilized for 10 min at room temperature in a 0.5% Triton X100 solution in PBS. Samples were then blocked for 2 h at room temperature in blocking buffer containing 1% BSA, 5% goat serum and 0.05% Tween20. Primary antibody at dilution 1:500 (chicken anti-βIII tubulin (NB100-1612, Novus) was incubated overnight at 4°C in blocking buffer. After 3 $\times$ 1-h washes in blocking buffer, samples were incubated with secondary antibody (1:500 goat anti-chicken Alexa647, Thermo Fisher Scientific, A-21449) for 3 h at room temperature.

2.14 | Statistical Analysis

GraphPad Prism v8.0 software (GraphPad Software, Inc. La Jolla, CA, USA) was used to produce graphs and to determine statistical significance. All data are presented as the mean ± standard deviation (SD). When comparing two groups, a Student's t-test was performed. When three or more groups were compared, One-way Analysis of Variance (ANOVA) was used to determine statistical significance, followed by a Tukey multiple comparisons

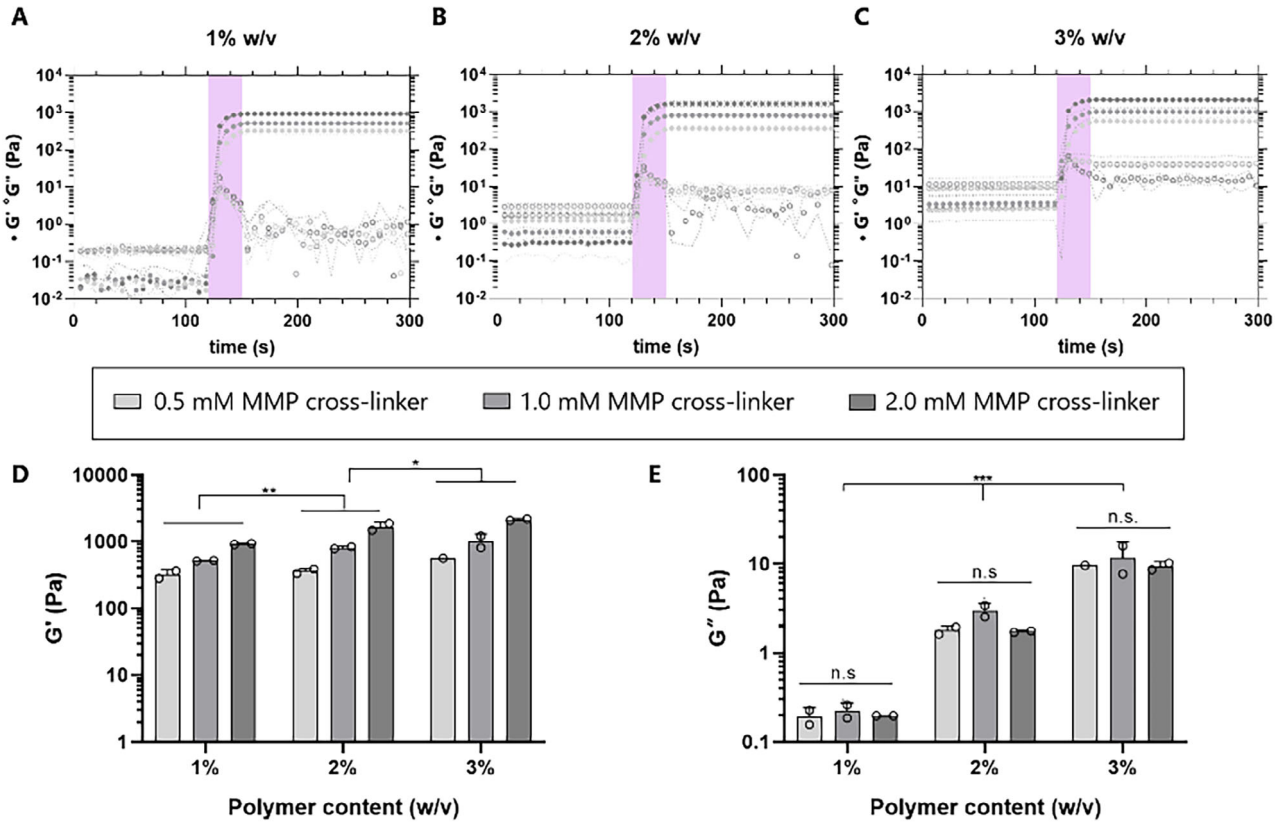

FIGURE 1 | Rheological assessment of hydrogels at (A) 1% w/v alginate-norbornene, (B) 2% w/v alginate-norbornene, and (C) 3% w/v alginate-norbornene, at crosslinking density of 0.5 mM, 1 mM and 2 mM. Purple shading indicates exposure to UV for 30 s to induce polymerization. Filled circles represent G', empty circles represent G". (D) G' post UV irradiation (n = 2); and (E) G" before UV irradiation (n = 2). *$p \leq 0.05$, **$p \leq 0.01$, ***$p \leq 0.001$.

test. Values were considered to be statistically significant when p < 0.05. Significance is highlighted as follows: *$p < 0.05$, **$p < 0.01$, ***$p < 0.001$, ****$p < 0.0001$.

3 | Results

3.1 | Effect of Polymer Density and Crosslinker Concentration on Rheological Properties

Alginate was functionalized with norbornene groups by DMTMM activation reaching a degree of functionalization of 7.1% determined by 1H NMR. An ideal polymer system for cell encapsulation should work in mild conditions and appropriate buffers, such as PBS or cell culture medium, as the system we present here. Crosslinking should happen on demand and in a short period of time to avoid cell sedimentation and ensure real 3D distribution. In order to investigate the gelation times, we turned to photo-rheology. Pre-gel solutions at 1, 2, and 3% w/v polymer, 0.5, 1, and 2 mM crosslinker, 2.5 mM thiol-RGD, and 2 mM LAP were loaded onto a photo-rheometer. RGD was included to obtain data relevant for cell experiments that followed. Figure 1 depicts the speed of crosslinking at the different polymer concentration and crosslinking concentrations tested (Figure 1A–C). A plateau in the storage moduli could be observed before the end of the 30 s irradiation period, portraying that thiol-ene chemistry is very fast compared to conventional ionic interactions in crosslinking the hydrogel. Cross-over of G' over G″ (often recorded as the gelation time) happened already after 6 s of irradiation, which was the first sampling point possible. At each polymer concentration, the effect of crosslinker concentration on final mechanical properties was evident. Additionally, the higher the crosslinker concentration, the higher the storage modulus (Figure 1D). Therefore, by modifying polymer concentration and/or crosslinker concentration, the hydrogels could range from very soft formulations (~320 Pa) to stiffer formulations (~2.1 kPa). All values are reported in Table 1. Higher crosslinker concentrations were not tested, as for subsequent applications we wanted to have free norbornene groups available. Polymer concentration had an important

TABLE 1 | Storage modulus of the different formulations by varying the polymer content (1, 2, and 3% w/v) and crosslinker concentration (0.5, 1, and 2 mM). Values shown as average ± standard deviation.

	1% w/v	2% w/v	3% w/v
0.5 mM crosslinker	323.2 ± 58.7 Pa	361.1 ± 35.3 Pa	559.0 Pa
1 mM crosslinker	516.0 ± 8.4 Pa	805.1 ± 40.3 Pa	1009 ± 281.7 Pa
2 mM crosslinker	924.7 ± 20.4 Pa	1669 ± 281.4 Pa	2125 ± 77.0 Pa

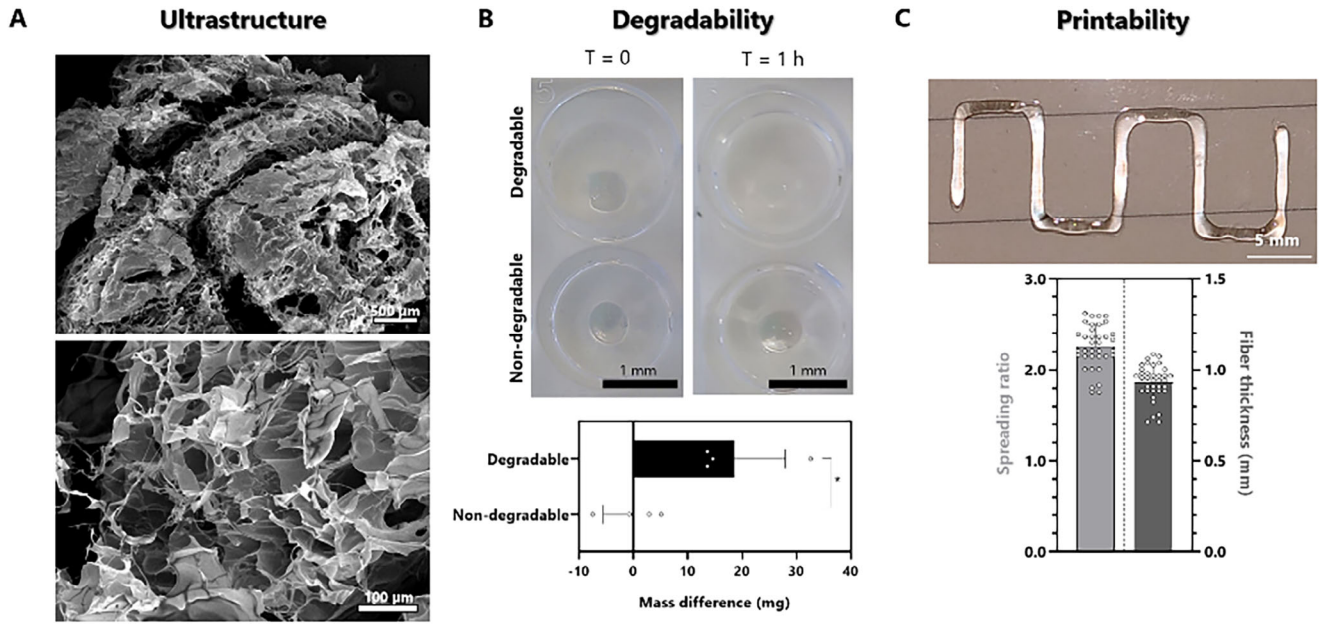

FIGURE 2 | Further characterization of developed acellular hydrogels. (A) Microstructure analyzed by SEM; (B) degradability testing of MMP-sequence crosslinker (degradable) vs PEG crosslinker (non-degradable), $*p \leq 0.05$ (n = 4); and (C) extrusion-based printability (n = 36) (C).

effect on the viscous component before crosslinking (loss modulus before UV exposure) (Figure 1E), while the crosslinker concentration did not have an influence. Values are presented in Table S1. This is somehow expected as the alginate-norbornene is a much larger molecule (~122 kg/mol) compared with the crosslinker (~1.5 kg/mol). This could allow to decouple mechanical properties from processing properties, for example those relevant for extrusion (bio)printing. while the amount of crosslinker was dominant for the final mechanical properties post-gelation.

3.2 | Ultrastructure, Swelling, Degradation, and Printability

Acellular hydrogels were snap-frozen, lyophilized, and sputter-coated for visualization in the SEM. Predominantly large porous structures were visible throughout the whole gels (Figure 2A). Next, we performed a swelling test. After 24 h in PBS at 37°C, the swollen gels were weighed and the swelling was calculated compared to their initial state (as cast). Gels crosslinked with the MMP-cleavable sequence were compared to their non-degradable counterpart, using a dithiolated PEG as control crosslinker. The degradable hydrogels (containing the MMP-crosslinker) were observed to swell to 306.0% ± 76.3% while the non-degradable hydrogels swelled less (226.4% ± 20.7%) (Figure S1). After this, we were interested to understand how quickly the MMP-degradable hydrogels degraded in the presence of an MMP-enzyme. Degradation tests were performed after swelling as above by incubation in collagenase I in PBS containing 0.36 mM $CaCl_2$ as enzyme co-factor. For fast visualization, hydrogels were incubated in high concentration collagenase (10 mg/mL) for 1 h at 37°C and pictures were taken. The degradable hydrogels had almost completely disappeared, while non-degradable hydrogels retained their shape (Figure 2B, top). A lower collagenase concentration (2 U/mL) was used to slow down the degradation and allow weighing the gels upon enzymatic treatment for 8 h. Quantitatively, degradable hydrogels had a loss of 18.6 mg ± 9.3 mg over the incubation period, while non-degradable gels presented a mass difference of 0.1 mg ± 5.5 mg (Figure 2B, bottom). These experiments confirmed that, indeed, the crosslinker used could be degraded by MMPs.

Bioprinting offers the possibility to position cells in a highly accurate manner to construct tissue mimics. Therefore, next, we wanted to confirm the printability of these degradable formulations using a standard extrusion-based printer. A pre-gel solution (4% w/v alginate-norbornene, crosslinker and photoinitiator) was loaded onto a 3 mL syringe and placed into a pressure-driven print-head. One layer consisting of 5 parallel vertical lines and 4 horizontal lines, making one continuous print was extruded and exposed to 30 s of UV light (Figure 2C top). Then, the quality of the print was assessed by image analysis. Fiber thickness was measured and determined to be 0.93 mm ± 0.10 mm. By using the inner diameter of the needle used (22 G, 0.41 mm), the spreading ratio was calculated to be 2.26 ± 0.24 (Figure 2C bottom).

3.3 | Alginate-Norbornene Hydrogels Support the Growth of Human Endometrial Organoids

Having benchmarked the effects of the formulation on the rheological properties, the enzymatic degradability and printability, we next sought out to understand how suitable of a matrix these remodelable systems were for several advanced cell types and organoids. First, we started with human endometrial organoids. Healthy human endometrial organoids were formed in Geltrex domes, harvested as small clusters and then encapsulated in 1% w/v, 0.5 mM MMP-cleavable crosslinker and 2.5 mM RGD hydrogels. The human endometrial organoids remained viable throughout the 7-day culture period (Figure 3A), as determined

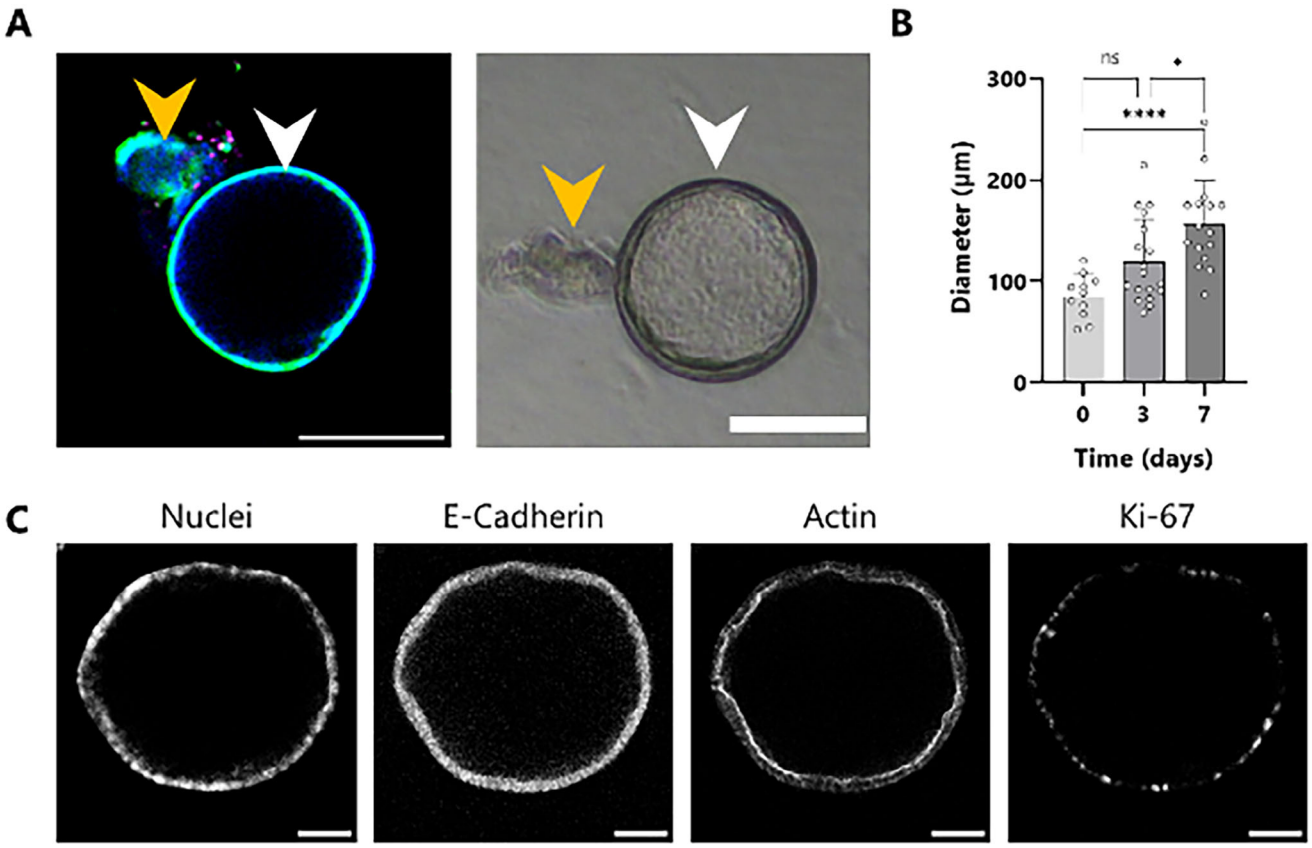

FIGURE 3 | Human endometrial organoids encapsulated in alginate-norbornene hydrogels at 1% w/v, 0.5 mM MMP-cleavable crosslinker, and 2.5 mM RGD. (A) Viability assay of organoids cultured for 7 days (left; blue = cell nuclei, green = live cells, magenta = dead cells) and under brightfield microscopy (right), where circular or elliptical shaped organoids are highly viable (white arrow) and irregular non-lumenized structures are less viable (yellow arrow); (B) Diameter of organoids over culture period (n = 11-18; $*p \leq 0.05$, $****p \leq 0.0001$, average ± standard deviation). (C) Immunostaining after 7 days in culture. All scale bars = 50 µm.

via live-dead staining. Fully formed organoids, hollow and round, did not contain dead cells (white arrow). Dead cells could be observed only as part of organoid debris. These structures did not have a circular shape (yellow arrow) and probably are derived from the splitting process. Endometrial organoids grew in size over time, from an average diameter of 85.3 µm ± 21.4 µm at day 0, up to 119.3 µm ± 41.8 µm at day 3 and 156.7 µm ± 42.8 µm at day 7 (Figure 3B). Organoids appeared smaller in alginate-norbornene compared to the ones grown in Geltrex, but the size difference was not significant. Notably, the size range in Geltrex was distributed wider (Figure S2). Cells in the organoids were proliferative, as seen by positive staining of Ki67, and expressed E-Cadherin showing cell-cell interactions and a correct epithelium phenotype (Figure 3C).

3.4 | Alginate-Norbornene Hydrogels Support the Growth of Mouse Thyroid Follicles

The next organ we ventured to replicate was the endocrine thyroid gland, which regulates metabolism, growth and development. Thyroid follicles were obtained from differentiation of mouse ESC into embryoid bodies and subsequently grown in Matrigel domes. Upon harvesting, thyroid follicles were encapsulated in gels with a composition of 1% alginate-norbornene, 1 mM MMP crosslinker and 2.5 mM RGD. The thyroid follicles encapsulated in the hydrogels presented the expected morphology presenting an internal lumen [38] after 4 days in culture (Figure 4A). Cell viability was high inside the gels, as very few ethidium homodimer-positive cells could be seen (Figure 4B). Most importantly, thyroid follicles expressed thyroglobulin (Tg) and mature thyroxine (T4) within the follicles (Figure 4C). The thyroid follicles presented proliferating cells (Ki67-positive cells) and showed a classical morphology with luminal structures (Figure 4D). Follicles grew significanlty in size over the culture period time (Figure 4E). At day 1 post-encapsulation, thyroid follicles presented an average long axis length of 194.6 µm ± 80.9 µm; while at day 4 the length of the long axis was of 325.0 µm ± 73.8 µm.

3.5 | Alginate-Norbornene Hydrogels Support the Growth of Mouse Intestinal Organoids

The last organoid model we tested in our hydrogel platform were mouse embryonic intestinal organoids. These were encapsulated in hydrogels consisting of 3% alginate-norbornene, 1 mM MMP crosslinker and 2.5 mM RGD. After 7 days in culture, the intestinal organoids presented a spherical morphology with an internal lumen, and the cells established a tight epithelial barrier, characterized by cohesive intercellular junctions as shown by the

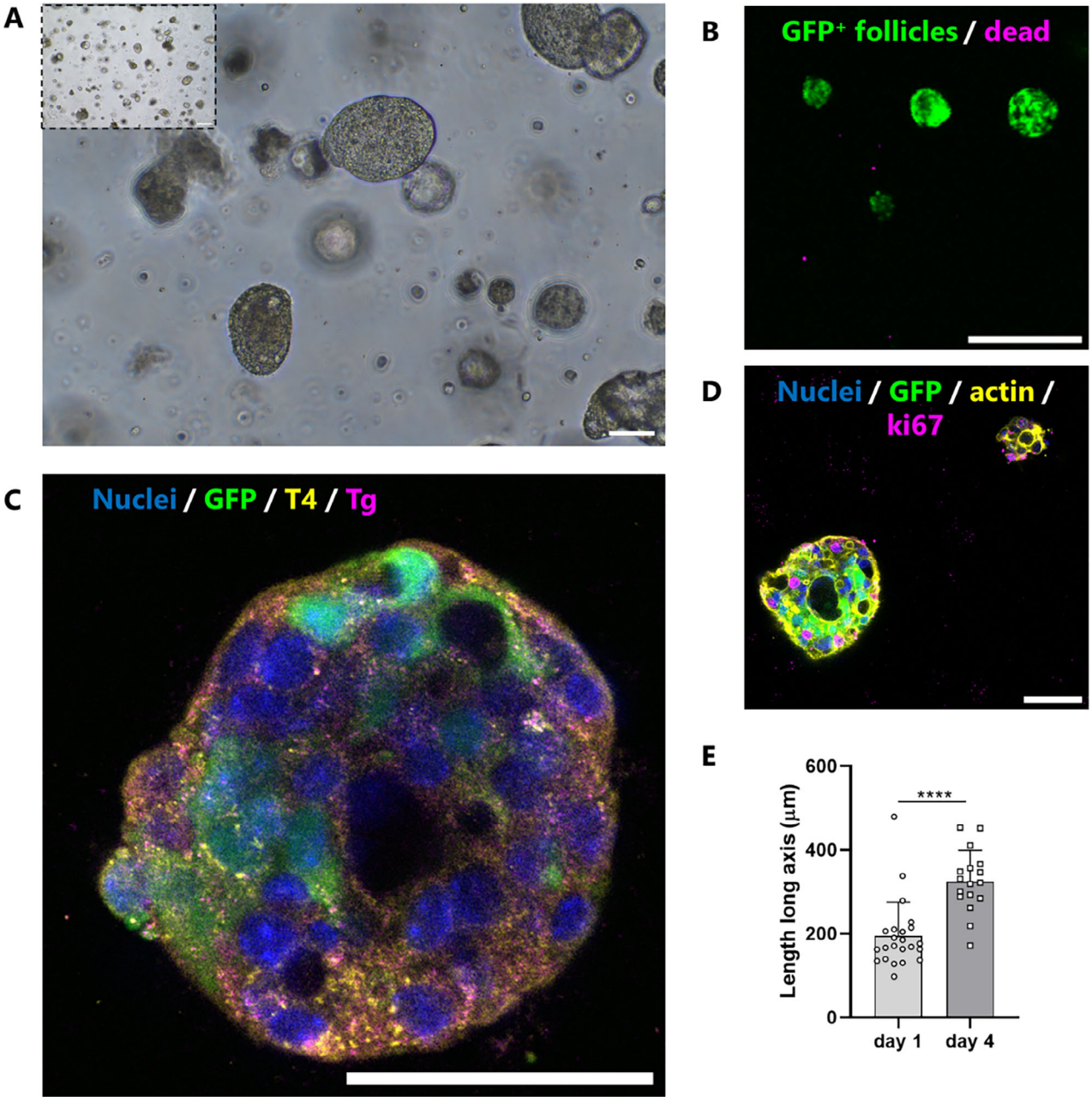

FIGURE 4 | Mouse ESC-derived thyroid follicles encapsulated in 1% w/v alginate-norbornene, 1 mM MMP-cleavable crosslinker and 2.5 mM RGD hydrogels after 4 days in culture present desired morphology under brightfield imaging (A) scale bar 200 µm, inset scale bar 500 µm; follicles present high cell viability after two days in culture (scale bar = 200 µm) (B); follicles express mature thyroid markers T4 and Tg (scale bar = 50 µm) (C); as well as proliferation marker Ki67 (scale bar = 50 µm) (D); follicles grow over time as determined by quantification of the long axis (****p< <0,0001, n = 17-23) (E).

expression of E-cadherin. Furthermore, the organoids showed a marked apical-basal polarity as seen by the localization of E-Cadherin on the basolateral side and an F-actin-rich brush border on the apical (lumen) side. The development and maintenance of such polarity is required for correct organoid function. The presence of Ki-67 positive cells indicated the presence of proliferative cells in the organoids (Figure 5). The embedded organoids remained spherical, with no branching or budding, which may indicate an early not yet differentiated stage.

3.6 | Alginate-Norbornene Hydrogels Support Vascularization Potential

Despite the pivotal role of vascularization in homeostasis and disease, inclusion of a vascular component in organotypic tissue models and organoids remains often a challenge. To evaluate the potential of our hydrogel system to produce higher complexity models, we tested its angiogenic potential. For this purpose, HUVECs and MSCs were encapsulated in 3% alginate-

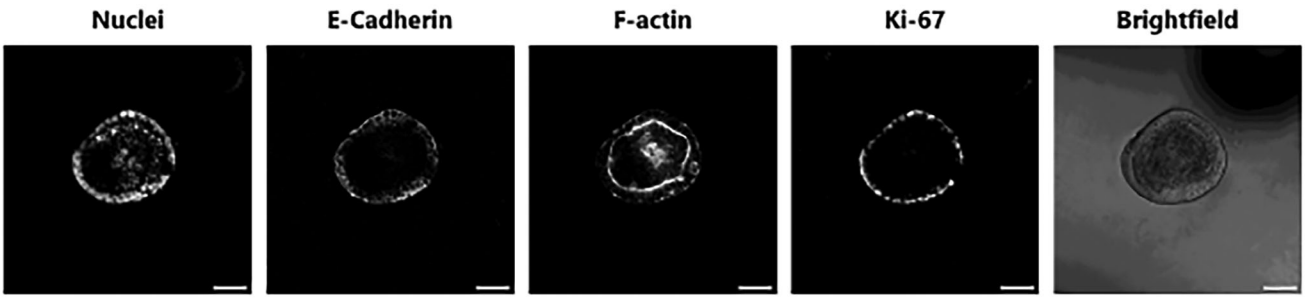

FIGURE 5 | Immunostaining of E-cadherin in mouse embryonic intestinal organoids cultured for 7 days inside alginate-norbornene hydrogels (3% alginate-norbornene, 1 mM MMP crosslinker and 2.5 mM RGD). All scale bars = 50 μm.

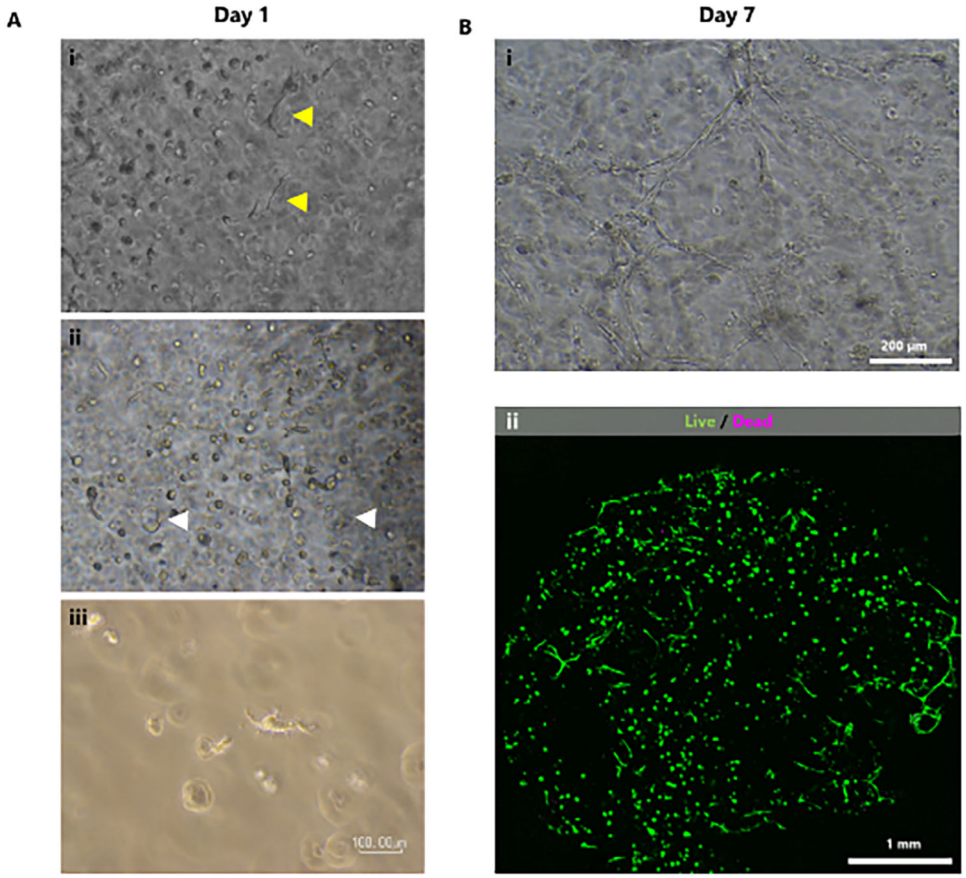

FIGURE 6 | Endothelial and supporting cells encapsulated as single cell suspension in alginate-norbornene hydrogels (3%, 1 mM MMP, 2.5 mM RGD). (A) After 1 day in culture, elongated cells (i), early vacuolation (ii) and tip cell morphology (iii) can be identified. (B) After 7 days in culture, an early vascular network formation was observed under brightfield microscopy (i), with high cell viability (ii).

norbornene hydrogels, 1 mM MMP crosslinker and 2.5 mM RGD. After one day in culture (Figure 6A), cell elongation was already visible (Figure 6A i), early signs of vacuolation could be observed (Figure 6A ii) and tip cell morphology with filopodia were identified (Figure 6A iii). After seven days in culture, some early networks could be recognized (Figure 6B i). The co-cultured cells encapsulated in the hydrogels presented high cell viability (Figure 6B ii) (>92%). Interestingly, when endothelial and support cells where cultured in non-degradable hydrogels (using PEG di-thiol as crosslinker) with RGD, the cells presented a rounded shape with barely any protrusions (Figure S3A), while remaining highly viable (Figure S3B). This seems to indicate that not only cell binding but also matrix degradability are essential for endothelial cell arrangement. Minimal binding sequences of other extracellular matrix proteins were also used at 2.5 mM. These included, apart from fibronectin RGD, YIGSR from laminin and GFOGER from collagen type 1. Similar initial cell attachment was seen in all formulations (Figure S4).

Another approach to organoid vascularization is the co-culture with endothelial cells in spheroids, which allow increased cell-cell contacts, an important feature for angiogenesis. Therefore, we embedded spheroids of HUVECs and MSCs obtained by the hanging drop method in 1% alginate-norbornene hydrogels,

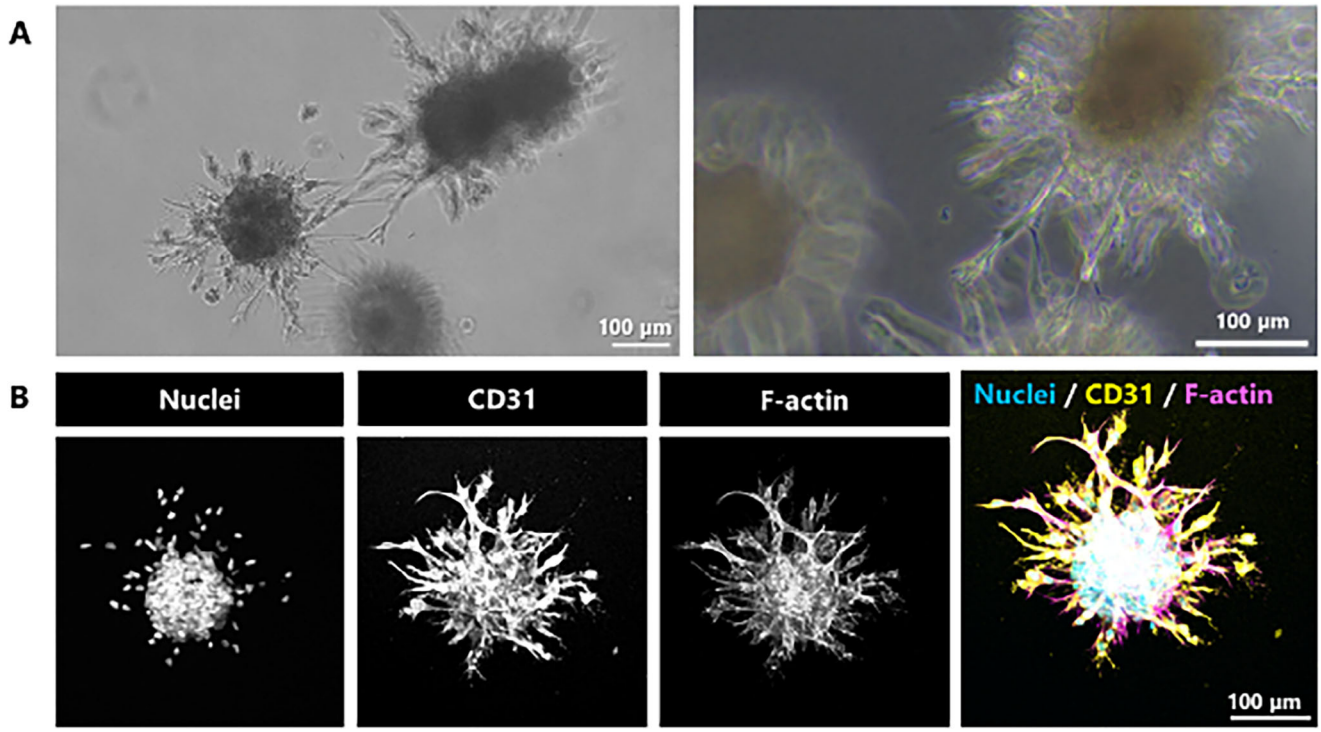

FIGURE 7 | Angiogenic sprouting of endothelial-mesenchymal spheroids encapsulated in 1% alginate-norbornene, 1 mM MMP crosslinker, and 2.5 mM RGD hydrogels after 24 h in culture, visualized with brightfield microscopy (A), and immunocytochemistry staining (B). All scale bars = 100 µm.

1 mM MMP crosslinker and 2.5 mM RGD. After only 24 h, clear sprouts and even contacts between adjacent spheroids were visible (Figure 7A). Increased and faster angiogenic sprouting was observed using spheroids compared to the single cell suspension approach. Not only the initial cell configuration but also the hydrogel formulation with a lower polymer content and softer mechanical properties could explain these findings. Upon staining for endothelial marker CD31, it could be seen that these sprouts were primarily from the HUVECs in the spheroids (Figure 7B).

3.7 | Alginate-Norbornene Hydrogels Support Innervation Potential

Innervation of 3D organotypic tissue models can increase complexity of such models, allowing the study of neurosensitive processes (e.g. pain). Therefore, iPSCs were differentiated into peripheral neurons, grown in neurospheres, and encapsulated in our hydrogel. A formulation of 1% alginate-norbornene, 1 mM MMP crosslinker, and 2.5 mM RGD was used. Cells were kept in culture for 7 days to allow neurite outgrowth. During this culture time, neurite outgrowth from the cell body and into the material could be observed. Different types of neurites were visible: multiple single projections (Figure 8A) and thicker neurite bundles (Figure 8B). These structures stained positive for the neural marker βIII-tubulin (Figure 8C) and showcase the formation of new neurites and more established outgrowth with the observed bundles. The length of neurites was quantified from brightfield images. The longest single projection measured was 517 µm. The average length was 253 µm, with a range from 76 to 517 µm. Furthermore, the hydrogels, while being soft, were robust enough to support these neurites without damaging them mechanically during normal culture procedures like media change or staining, and imaging.

4 | Discussion

This work showcases the use of a hydrogel platform based on MMP-degradable norbornene-functionalized alginate for the growth of a variety of organoids, which can potentially be vascularized and innervated. Mechanical properties, degradability and cell adhesion can be tuned, offering the potential of use in tandem with biofabrication technologies.

Alginate is a bioinert material and thus needs to be modified to allow cell binding. In the current body of work, all formulations included RGD. Many studies have used RGD as a binding site [42]. We have demonstrated that the system also works with other cell-binding peptides (GFOGER and YIGSR) when a terminal cysteine is present. As the scope of this study was to examine the possibility of using this system for a wide variety of cell types, we used the "universal" RGD integrin binding domain. Depending on the application and research question, the choice of ECM-mimicking peptides is crucial. For example, early work from Ali and colleagues showed improved endothelial network formation when RGD was combined with YIGSR in PEG-diacrylate hydrogels crosslinked with MMP-cleavable linkers [43]. Human intestinal organoids presented increased viability when RGD was presented, compared to GFOGER and IKVAV in 4-arm PEG-maleimide hydrogels crosslinked with MMP-cleavable linkers [44]. However, in 8-arm PEG hydrogels, GFOGER was superior than RGD for the formation and growth of human enteroids

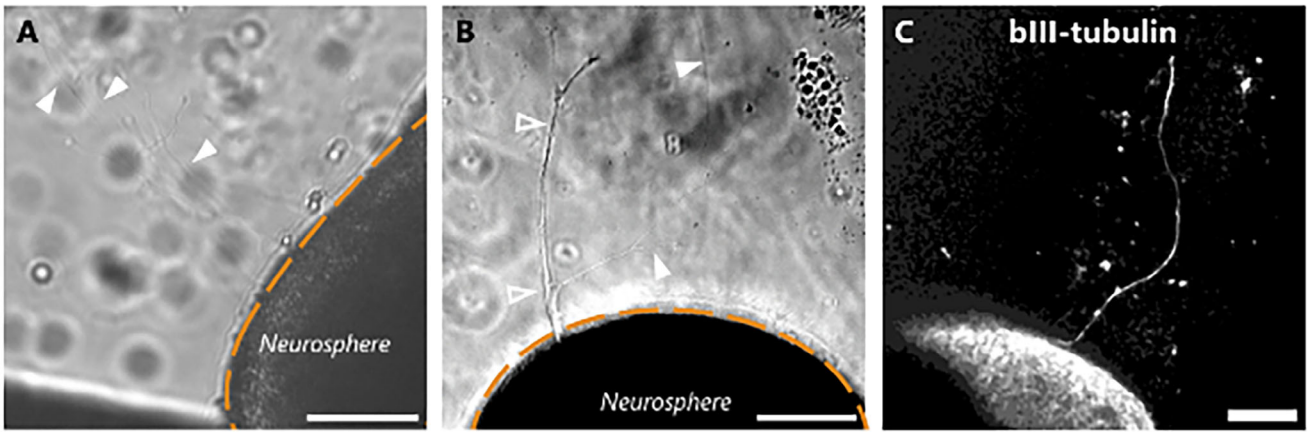

FIGURE 8 | Human neurospheres from induced pluripotent stem cells encapsulated in alginate-norbornene hydrogels at 1% w/v, 1 mM MMP-cleavable crosslinker, and 2.5 mM RGD. (A) Thin and small axons (filled arrow heads) invade the hydrogel coming from the neurosphere (orange dashed line); (B) Thick branching axons (empty arrow heads), and thin and small axons (filled arrow heads) invade the hydrogel coming from the neurosphere (orange dashed line); (C) Immunostaining for bIII-tubulin after 8 days in culture. All scale bars = 100 μm.

(intestinal organoids) [45]. In our work, by only using RGD neurite outgrowth was achieved. It could be expected that by using more brain-like ECM peptides, this outgrowth could be increased. Laminin-mimetic IKVAV has been shown to improve neurogenesis on 2D hydrogels in vitro [46]. Peptides based on collagen IV [47] might also improve axonal outgrowth as so does the whole protein [48]. Endometrial organoids could grow and presented proliferative cells in gels with RGD, similar to our work, albeit GFOGER promoting enhanced organoid growth [45].

Because the impact of introducing enzymatic degradability into our system was so great in single endothelial cell suspension, all formulations used for all other cultures used the MMP-cleavable sequence as crosslinker. In this study the VPLS↓LYSG sequence was used, which can be cleaved by MMP2 and MMP5 [49]. Many studies using synthetic hydrogels use MMP2/9 sequence known as PQ [GPQG↓IWGQ] [42, 50]. The use of a modified PQ sequence [CGPQG↓PAGQGCR] with a lower degradation rate, showed a change in angiogenic sprouting, with lower invasion speed but higher collective migration behavior in methacrylated dextran hydrogels [51]. Inversely, a faster degrading sequence than PQ is VPM [VPMS↓MRGG]. In 4-arm PEG vinyl sulfone hydrogels, endothelial and supportive fibroblasts spread out faster when VPM was used compared to PQ [52]. Lueckgen and colleagues also reported similar findings to ours, where fibroblast spreading and elongation was only present when using MMP-cleavable crosslinking sequences, even in the presence of RGD motifs in an alginate-norbornene system [53]. Matrix degradability has been shown to impact the growth of enteroids, while in non-degradable matrices organoids remained smaller [45].

This current work showed the ability to tune the mechanical properties in a straightforward manner, by either modifying the polymer content and/or changing the crosslinker concentration. Notably, and not shown often in the literature, we were able to show that the substoichiometric crosslinker concentration dictated the stiffness of the post-crosslinked gel, while the polymer concentration dictated the viscosity of the gel precursor. This is an interesting strategy to decouple final mechanical properties (important for cellular behavior) from viscosity of the precursor (important for processing and bioprinting). This observation is important for further study to see if it is a general trend in the field that can be leveraged.

The range of obtained shear moduli (~300–~2100 Pa) was targeted for soft tissues and cells which are standardly cultured in Matrigel (330–~400 Pa [41, 54]). The most used formulation in this study was 1% w/v alginate-norbornene and 1 mM cell-degradable cross-linker, as that yielded very soft hydrogels, yet easily handleable. At lower cross-linker concentrations hydrogels were challenging to manipulate, although not impossible, as the endometrial organoids were cultured in hydrogels with this composition. For studies focusing on tissues requiring higher stiffness, the polymer content and crosslinker concentration could be increased.

The system presented here is initially purely elastic as the hydrogel is formed of static covalent bonds. The gels are expected to soften locally over time by the secretion of MMPs by the cells. Simultaneously, however, cells are expected to secrete their own ECM and thus reorganization of the material would occur. Upon deposition of newly synthesized ECM, the hydrogel would become viscoelastic. Further work could focus on engineering the viscoelasticity of the hydrogel platform to better mimic tissues [55]. Approaches for this could include norbornene-functionalization of oxidized alginate (containing aldehyde groups) [23] and a dual use of crosslinkers, dihydrazide and cysteine-flanked MMP sequences. This would presumably render gels with stress-relaxation properties as we have shown previously for hydrazone and oxime crosslinking in oxidized alginate [23]. Incorporation of supramolecular chemistry could also be an option to introduce viscoelasticity. UPy moieties [56] or host-guest molecules [57] could be easily grafted onto the alginate-norbornene via terminal thiols. Norbornene has been used to crosslink alginate hydrogels and also offer tunable handles for modifying stress relaxation [58]. A cysteine-modified alginate system has been reported by which thiol protection can be enzymatically released on demand to be subsequently used for crosslinking or moiety grafting [58].

The hydrogel system presented in this work renders itself valuable in the biofabrication field. We have demonstrated the possibility of extrusion bioprinting. Yet, our hydrogels could be amenable to all light-based biofabrication techniques, including DLP [59], multiphoton [60] and volumetric bioprinting [61–63]. Local and temporal control of crosslinks, or peptide presentation could also be performed. Others have shown the possibility of photopatterning alginate hydrogels with areas of different stiffness and degradation profile [64]. We have also shown grafting of RGD in a localized manner with the use of photomasks [29]. Multiphoton lithography enables the grafting in a highly precise manner [65, 66]. Moreover, other interesting biological cues, such as growth factor-mimicking peptides, could be easily grafted in bulk or in a localized manner. For example, the so-called QK peptide (KLTWQELYQLKYKGI) is a VEGF-mimicking sequence [67] that can improve vascularization outcomes in vitro and in vivo [68]. It has been functionalized onto alginate [69, 70] and in self-assembled hydrogels based on elastin-like recombinamers [71].

We have shown here how the basic formulations of this system can support the growth, differentiation and phenotype of a variety of organoids, including intestinal, endometrial and thyroid. The organs these organoids recapitulate are heavily vascularized and innervated. Therefore, developing a material that also supports endothelial cell sprouting and neurite outgrowth is paramount. It has been recently demonstrated that organoids can be developed to contain vasculature [72], but co-culture with endothelial cells is a slightly more straight-forward and universal approach [73]. It has been shown that thyroid follicles produce more T4 and respond more physiologically to endocrine disruptors in presence of fluid flow in an organ-on-chip device [38, 74]. Thyroid spheroids bioprinted next to allantoid spheroids in collagen gels showed apical polarization and maturation, enhanced by the endothelial cells coming from the allantoid compartment [75]. It can be hypothesized that combining thyroid follicles with endothelial cells in the present hydrogel would also promote their further maturation and marker expression. Innervation of tissue engineered constructs remains an understudied field, despite its crucial function in all organs [76]. Previous work in our group demonstrated the interaction of neurites from neurospheres with endometrial organoids derived from an endometrial adenocarcinoma cell line, albeit using Matrigel and fibrin gels [77]. Therefore, in our future work we aim to explore the co-culture of the vascular and neural component with endometrial organoids derived from patients with endometriosis to study pain processes in a more physiological model using our hydrogel platform.

In summary, this work presents a versatile and innovative material for the 3D culture of organotypic tissue models. Synthesis of the alginate-norbornene is relatively straightforward and the rest of components of this system are commercially available. These hydrogels can be easily adopted by researchers who are not material scientists, as it is an in-one-pot fabrication method. The formulations presented in this work are rather simple, but can be optimized for each cell type, in terms of crosslinker, ECM ligand, and stiffness. Importantly, tissue models with increased complexity can eventually be obtained by the incorporation of vascularization and innervation. Furthermore, the use of these inks with high resolution light-based biofabrication techniques can allow the development of organotypic tissue models with spatial and temporal control of physical and/or chemical cues. This platform holds the potential to become a substitute to traditional culture in Matrigel.

Acknowledgements

This work was supported by the partners of Regenerative Medicine Crossing Borders (RegMed XB), a public–private partnership that uses regenerative medicine strategies to cure common chronic diseases. This collaboration project is financed by the Dutch Ministry of Economic Affairs by means of the PPP Allowance made available by the Top Sector Life Sciences & Health to stimulate public–private partnerships. This study was also financially supported by the European Union's Horizon 2020 Research and Innovation Programme under grant agreement no. 825745 (SCREENED).

Conflicts of Interest

The authors declare no conflicts of interest.

Data Availability Statement

The data that support the findings of this study are available from the corresponding author upon reasonable request.

References

1. J. Kim, B.-K. Koo, and J. A. Knoblich, "Human Organoids: Model Systems for Human Biology and Medicine," *Nature Reviews Molecular Cell Biology* 21, no. 10 (2020): 571–584, https://doi.org/10.1038/s41580-020-0259-3.

2. K. Schneeberger, B. Spee, P. Costa, N. Sachs, H. Clevers, and J. Malda, "Converging Biofabrication and Organoid Technologies: the next Frontier in Hepatic and Intestinal Tissue Engineering?," *Biofabrication* 9 (1) (2017): 013001, https://doi.org/10.1088/1758-5090/aa6121.

3. Z. Li, L. Chen, J. Wu, et al., "A Review of 3D Bioprinting for Organoids," *Medical Review* 5, no. 4 (2025): 318–338, https://doi.org/10.1515/mr-2024-0089.

4. P. Kakni, R. Truckenmüller, P. Habibović, and S. Giselbrecht, "Challenges to, and Prospects for, Reverse Engineering the Gastrointestinal Tract Using Organoids," *Trends in Biotechnology* 40, no. 8 (2022): 932–944, https://doi.org/10.1016/j.tibtech.2022.01.006.

5. J. F. van Sprang, J. G. M. Aarts, M. G. T. A. Rutten, et al., "Co-Assembled Supramolecular Hydrogelators Enhance Glomerulogenesis in Kidney Organoids through Cell-Adhesive Motifs," *Advanced Functional Materials* 34, no. 42 (2024): 2404786, https://doi.org/10.1002/adfm.202404786.

6. J. S. Gnecco, A. Brown, K. Buttrey, et al., "Organoid Co-Culture Model of the Human Endometrium in a Fully Synthetic Extracellular Matrix Enables the Study of Epithelial-Stromal Crosstalk," *Med* 4 (2023): 554–579.e9, https://doi.org/10.1016/j.medj.2023.07.004.

7. V. U. Buck, B. Gellersen, R. E. Leube, and I. Classen-Linke, "Interaction of Human Trophoblast Cells with Gland-Like Endometrial Spheroids: a Model System for Trophoblast Invasion," *Human Reproduction* 30, no. 4 (2015): 906–916, https://doi.org/10.1093/humrep/dev011.

8. R. W. Orkin, P. Gehron, E. B. McGoodwin, G. R. Martin, T. Valentine, and R. A. M. Swarm, "A Murine Tumor Producing a Matrix of Basement Membrane," *The Journal of Experimental Medicine* 145, no. 1 (1977): 204–220, https://doi.org/10.1084/jem.145.1.204.

9. H. K. Kleinman, M. L. McGarvey, J. R. Hassell, et al., "Basement Membrane Complexes with Biological Activity," *Biochemistry* 25, no. 2 (1986): 312–318, https://doi.org/10.1021/bi00350a005.

10. E. A. Aisenbrey and W. L. Murphy, "Synthetic Alternatives to Matrigel," *Nature Reviews Materials* 5, no. 7 (2020): 539–551, https://doi.org/10.1038/s41578-020-0199-8.

11. A. S. Sawhney, C. P. Pathak, J. J. van Rensburg, R. C. Dunn, and J. A. Hubbell, "Optimization of Photopolymerized Bioerodible Hydrogel Properties for Adhesion Prevention," *Journal of Biomedical Materials Research* 28, no. 7 (1994): 831–838, https://doi.org/10.1002/jbm.820280710.

12. C.-C. Lin, A. Raza, and H. Shih, "PEG Hydrogels Formed by Thiol-Ene Photo-Click Chemistry and Their Effect on the Formation and Recovery of Insulin-Secreting Cell Spheroids," *Biomaterials* 32, no. 36 (2011): 9685–9695, https://doi.org/10.1016/j.biomaterials.2011.08.083.

13. M. V. Tsurkan, K. Chwalek, S. Prokoph, et al., "Defined Polymer–Peptide Conjugates to Form Cell-Instructive starPEG–Heparin Matrices in Situ," *Advanced Materials* 25, no. 18 (2013): 2606–2610, https://doi.org/10.1002/adma.201300691.

14. J. Fernández-Pérez, M. Binner, C. Werner, and L. J. Bray, "Limbal Stromal Cells Derived from Porcine Tissue Demonstrate Mesenchymal Characteristics in Vitro," *Scientific Reports* 7, no. 1 (2017): 6377, https://doi.org/10.1038/s41598-017-06898-2.

15. M. P. Lutolf and J. A. Hubbell, "Synthesis and Physicochemical Characterization of End-Linked Poly(Ethylene Glycol)-Co-Peptide Hydrogels Formed by Michael-Type Addition," *Biomacromolecules* 4, no. 3 (2003): 713–722, https://doi.org/10.1021/bm025744e.

16. Y. Park, M. P. Lutolf, J. A. Hubbell, E. B. Hunziker, and M. Wong, "Bovine Primary Chondrocyte Culture in Synthetic Matrix Metalloproteinase-Sensitive Poly(Ethylene Glycol)-Based Hydrogels as a Scaffold for Cartilage Repair," *Tissue Engineering* 10 (2004): 515–522, https://doi.org/10.1089/107632704323061870.

17. M. Ehrbar, S. C. Rizzi, R. G. Schoenmakers, et al., "Biomolecular Hydrogels Formed and Degraded via Site-Specific Enzymatic Reactions," *Biomacromolecules* 8 (2007): 3000–3007, https://doi.org/10.1021/bm070228f.

18. T. J. Klein, S. C. Rizzi, K. Schrobback, et al., "Long-term Effects of Hydrogel Properties on human Chondrocyte Behavior," *Soft Matter* 6 (2010): 5175–5183, https://doi.org/10.1039/C0SM00229A.

19. C. Lubich, P. Allacher, M. de la Rosa, et al., "The Mystery of Antibodies against Polyethylene Glycol (PEG)—What Do We Know?," *Pharmaceutical Research* 33, no. 9 (2016): 2239–2249, https://doi.org/10.1007/s11095-016-1961-x.

20. Q. Yang, T. M. Jacobs, J. D. McCallen, et al., "Analysis of Pre-Existing IgG and IgM Antibodies against Polyethylene Glycol (PEG) in the General Population," *Analytical Chemistry* 88, no. 23 (2016): 11804–11812, https://doi.org/10.1021/acs.analchem.6b03437.

21. Y. Ju, W. S. Lee, E. H. Pilkington, et al., "Anti-PEG Antibodies Boosted in Humans by SARS-CoV-2 Lipid Nanoparticle mRNA Vaccine," *ACS Nano* 16 (2022): 11769–11780, https://doi.org/10.1021/acsnano.2c04543.

22. Y. Deng, A. Shavandi, O. V. Okoro, and L. Nie, "Alginate Modification via Click Chemistry for Biomedical Applications," *Carbohydrate Polymers* 270 (2021): 118360, https://doi.org/10.1016/j.carbpol.2021.118360.

23. F. L. C. Morgan, J. Fernández-Pérez, L. Moroni, and M. B. Baker, "Tuning Hydrogels by Mixing Dynamic Cross-linkers: Enabling Cell-instructive Hydrogels and Advanced Bioinks," *Advanced Healthcare Materials* 11 (2021): 2101576, https://doi.org/10.1002/adhm.202101576.

24. O. Jeon, K. H. Bouhadir, J. M. Mansour, and E. Alsberg, "Photocrosslinked Alginate Hydrogels with Tunable Biodegradation Rates and Mechanical Properties," *Biomaterials* 30, no. 14 (2009): 2724–2734, https://doi.org/10.1016/j.biomaterials.2009.01.034.

25. M. I. Neves, M. V. Magalhães, S. J. Bidarra, L. Moroni, and C. C. Barrias, "Versatile Click Alginate Hydrogels with Protease-Sensitive Domains as Cell Responsive/Instructive 3D Microenvironments," *Carbohydrate Polymers* 320 (2023): 121226, https://doi.org/10.1016/j.carbpol.2023.121226.

26. M. V. Magalhães, N. Débera, R. F. Pereira, M. I. Neves, C. C. Barrias, and S. J. Bidarra, "In Situ Crosslinkable Multi-Functional and Cell-Responsive Alginate 3D Matrix via Thiol-Maleimide Click Chemistry, "*Carbohydrate Polymers* 337 (2024): 122144, https://doi.org/10.1016/j.carbpol.2024.122144.

27. H. W. Ooi, J. M. M. Kocken, F. L. C. Morgan, et al., "Multivalency Enables Dynamic Supramolecular Host–Guest Hydrogel Formation," *Biomacromolecules* 21, no. 6 (2020): 2208–2217, https://doi.org/10.1021/acs.biomac.0c00148.

28. H. W. Ooi, C. Mota, A. Tessa Ten Cate, A. Calore, L. Moroni, and M. B. Baker, "Thiol–Ene Alginate Hydrogels as Versatile Bioinks for Bioprinting," *Biomacromolecules* 19, no. 8 (2018): 3390–3400, https://doi.org/10.1021/acs.biomac.8b00696.

29. A. J. Feliciano, R. Grant, J. Fernández-Pérez, S. Giselbrecht, and M. B. Baker, "Introducing Dynamicity: Engineering Stress Relaxation into Hydrogels via Thiol-Ene Modified Alginate for Mechanobiological in Vitro Modeling of the Cornea," *Macromolecular Bioscience* 24, no. 1 (2024): 2300109, https://doi.org/10.1002/mabi.202300109.

30. M. I. Neves, L. Moroni, and C. C. Barrias, "Modulating Alginate Hydrogels for Improved Biological Performance as Cellular 3D Microenvironments," *Frontiers in Bioengineering and Biotechnology* 8 (2020): 00665, https://doi.org/10.3389/fbioe.2020.00665.

31. R. F. Pereira, C. C. Barrias, P. J. Bártolo, and P. L. Granja, "Cell-Instructive Pectin Hydrogels Crosslinked via Thiol-Norbornene Photo-Click Chemistry for Skin Tissue Engineering," *Acta Biomaterialia* 66 (2018): 282–293, https://doi.org/10.1016/j.actbio.2017.11.016.

32. A. Cirulli, L. N. Borgheti-Cardoso, N. Torras, and E. Martínez, "Mimicking Human Skin Constructs Using Norbornene-Pullulan-Based Hydrogels," *International Journal of Bioprinting* 10, no. 4 (2024): 3395, https://doi.org/10.36922/ijb.3395.

33. A. Zengin, F. C. Teixeira, T. Feliciano, et al., "Matrix Metalloproteinase Degradable, In Situ Photocrosslinked Nanocomposite Bioinks for Bioprinting Applications," *Biomaterials Advances* 154 (2023): 213647, https://doi.org/10.1016/j.bioadv.2023.213647.

34. T. Geuens, F. A. A. Ruiter, A. Schumacher, et al., "Thiol-Ene Cross-Linked Alginate Hydrogel Encapsulation Modulates the Extracellular Matrix of Kidney Organoids by Reducing Abnormal Type 1a1 Collagen Deposition," *Biomaterials* 275 (2021): 120976, https://doi.org/10.1016/j.biomaterials.2021.120976.

35. F. Perin, A. Ricci, S. Fagiolino, et al., "Bioprinting of Alginate-Norbornene Bioinks to Create a Versatile Platform for Kidney in Vitro Modeling," *Bioactive Materials* 49 (2025): 550–563, https://doi.org/10.1016/j.bioactmat.2025.03.010.

36. M. Y. Turco, L. Gardner, J. Hughes, et al., "Long-term, Hormone-responsive Organoid Cultures of human Endometrium in a Chemically Defined Medium," *Nature Cell Biology* 19 (2017): 568–577, https://doi.org/10.1038/ncb3516.

37. M. Boretto, B. Cox, M. Noben, et al., "Development of Organoids from Mouse and Human Endometrium Showing Endometrial Epithelium Physiology and Long-Term Expandability," *Development (Cambridge, England)* 144 (2017): 1775–1786, https://doi.org/10.1242/dev.148478.

38. D. J. Carvalho, A. M. Kip, M. Romitti, et al., "Thyroid-on-a-Chip: an Organoid Platform for in Vitro Assessment of Endocrine Disruption," *Advanced Healthcare Materials* 12, no. 8 (2023): 2201555, https://doi.org/10.1002/adhm.202201555.

39. F. Antonica, D. F. Kasprzyk, R. Opitz, et al., "Generation of Functional Thyroid from Embryonic Stem Cells," *Nature* 491, no. 7422 (2012): 66–71, https://doi.org/10.1038/nature11525.

40. P. Kakni, R. Hueber, K. Knoops, et al., "Intestinal Organoid Culture in Polymer Film-Based Microwell Arrays," *Advanced Biosystems* 4, no. 10 (2020): 2000126, https://doi.org/10.1002/adbi.202000126.

41. S. M. Chambers, C. A. Fasano, E. P. Papapetrou, M. Tomishima, M. Sadelain, and L. Studer, "Highly Efficient Neural Conversion of Human ES and iPS Cells by Dual Inhibition of SMAD Signaling," *Nature Biotechnology* 27, no. 3 (2009): 275–280, https://doi.org/10.1038/nbt.1529.

42. C. Ligorio and A. Mata, "Synthetic Extracellular Matrices with Function-Encoding Peptides," *Nature Reviews Bioengineering* 1 (2023): 518–536, https://doi.org/10.1038/s44222-023-00055-3.

43. S. Ali, J. E. Saik, D. J. Gould, M. E. Dickinson, and J. L. West, "Immobilization of Cell-Adhesive Laminin Peptides in Degradable PEGDA Hydrogels Influences Endothelial Cell Tubulogenesis," *BioResearch Open Access* 2, no. 4 (2013): 241–249, https://doi.org/10.1089/biores.2013.0021.

44. R. Cruz-Acuña, M. Quirós, A. E. Farkas, et al., "Synthetic Hydrogels for Human Intestinal Organoid Generation and Colonic Wound Repair," *Nature Cell Biology* 19, no. 11 (2017): 1326–1335, https://doi.org/10.1038/ncb3632.

45. V. Hernandez-Gordillo, T. Kassis, A. Lampejo, et al., "Fully Synthetic Matrices for in vitro Culture of Primary Human Intestinal Enteroids and Endometrial Organoids," *Biomaterials* 254 (2020): 120125, https://doi.org/10.1016/j.biomaterials.2020.120125.

46. A. Farrukh, F. Ortega, W. Fan, et al., "Bifunctional Hydrogels Containing the Laminin Motif IKVAV Promote Neurogenesis," *Stem Cell Reports* 9, no. 5 (2017): 1432–1440, https://doi.org/10.1016/j.stemcr.2017.09.002.

47. M. K. Chelberg, J. B. McCarthy, A. P. Skubitz, L. T. Furcht, and E. C. Tsilibary, "Characterization of a Synthetic Peptide from Type IV Collagen That Promotes Melanoma Cell Adhesion, Spreading, and Motility," *The Journal of Cell Biology* 111, no. 1 (1990): 261–270, https://doi.org/10.1083/jcb.111.1.261.

48. C. O'Connor, I. Woods, S. F. McComish, et al., "Biomimetic Scaffolds Enhance iPSC Astrocyte Progenitor Angiogenic, Immunomodulatory, and Neurotrophic Capacity in a Stiffness and Matrix-Dependent Manner for Spinal Cord Repair Applications," *Advanced Healthcare Materials* 14, no. 16 (2025): 2500830, https://doi.org/10.1002/adhm.202500830.

49. J. Patterson and J. A. Hubbell, "Enhanced Proteolytic Degradation of Molecularly Engineered PEG Hydrogels in Response to MMP-1 and MMP-2," *Biomaterials* 31, no. 30 (2010): 7836–7845, https://doi.org/10.1016/j.biomaterials.2010.06.061.

50. V. L. Thai, D. O. Candelas, and J. K. Leach, "Tuning the Microenvironment to Create Functionally Distinct Mesenchymal Stromal Cell Spheroids," *Annals of Biomedical Engineering* 51, no. 7 (2023): 1558–1573, https://doi.org/10.1007/s10439-023-03162-9.

51. B. Trappmann, B. M. Baker, W. J. Polacheck, C. K. Choi, J. A. Burdick, and C. S. Chen, "Matrix Degradability Controls Multicellularity of 3D Cell Migration," *Nature Communications* 8 (2017): 371, https://doi.org/10.1038/s41467-017-00418-6.

52. M. Vigen, J. Ceccarelli, and A. J. Putnam, "Protease-Sensitive PEG Hydrogels Regulate Vascularization in Vitro and in Vivo," *Macromolecular Bioscience* 14, no. 10 (2014): 1368–1379, https://doi.org/10.1002/mabi.201400161.

53. A. Lueckgen, D. S. Garske, A. Ellinghaus, D. J. Mooney, G. N. Duda, and A. Cipitria, "Enzymatically-Degradable Alginate Hydrogels Promote Cell Spreading and in Vivo Tissue Infiltration," *Biomaterials* 217 (2019): 119294, https://doi.org/10.1016/j.biomaterials.2019.119294.

54. S. S. Soofi, J. A. Last, S. J. Liliensiek, P. F. Nealey, and C. J. Murphy, "The Elastic Modulus of Matrigel™ as Determined by Atomic Force Microscopy," *Journal of Structural Biology* 167 (2009): 216–219, https://doi.org/10.1016/j.jsb.2009.05.005.

55. O. Chaudhuri, J. Cooper-White, P. A. Janmey, D. J. Mooney, and V. B. Shenoy, "Effects of Extracellular Matrix Viscoelasticity on Cellular Behaviour," *Nature* 584, no. 7822 (2020): 535–546, https://doi.org/10.1038/s41586-020-2612-2.

56. M. Guo, L. M. Pitet, H. M. Wyss, M. Vos, P. Y. W. Dankers, and E. W. Meijer, "Tough Stimuli-Responsive Supramolecular Hydrogels with Hydrogen-Bonding Network Junctions," *Journal of the American Chemical Society* 136, no. 19 (2014): 6969–6977, https://doi.org/10.1021/ja500205v.

57. C. Loebel, C. B. Rodell, M. H. Chen, and J. A. Burdick, "Shear-Thinning and Self-Healing Hydrogels as Injectable Therapeutics and for 3D-Printing," *Nature Protocols* 12, no. 8 (2017): 1521–1541, https://doi.org/10.1038/nprot.2017.053.

58. S. Naeimipour, F. R. Boroojeni, P. Lifwergren, R. Selegård, and D. Aili, "Multimodal and Dynamic Cross-Linking of Modular Thiolated Alginate-Based Bioinks," *Materials Today Advances* 19 (2023): 100415, https://doi.org/10.1016/j.mtadv.2023.100415.

59. M. Zanon, L. Montalvillo-Jiménez, R. Cue-López, et al., "Vat 3D Printing of Full-Alginate Hydrogels *via* Thiol–Ene Reactions towards Tissue Engineering Applications," *Polymer Chemistry* 14 (42), (2023): 4856–4868, https://doi.org/10.1039/D3PY00902E.

60. D. M. Zuev, A. K. Nguyen, V. I. Putlyaev, and R. J. Narayan, "3D Printing and Bioprinting Using Multiphoton Lithography," *Bioprinting* 20 (2020): 00090, https://doi.org/10.1016/j.bprint.2020.e00090.

61. P. N. Bernal, P. Delrot, D. Loterie, et al., "Volumetric Bioprinting of Complex Living-Tissue Constructs within Seconds," *Advanced Materials* 31, no. 42 (2019): 1904209, https://doi.org/10.1002/adma.201904209.

62. R. Rizzo, D. Ruetsche, H. Liu, and M. Zenobi-Wong, "Optimized Photoclick (Bio)Resins for Fast Volumetric Bioprinting," *Advanced Materials* 33, no. 49 (2021): 2102900, https://doi.org/10.1002/adma.202102900.

63. N. Pien, B. Bogaert, M. Meeremans, et al., "Exploring the Impact of Volumetric Additive Manufacturing of Photo-Crosslinkable Gelatin on Mesenchymal Stromal Cell Behavior and Differentiation," *Additive Manufacturing* 109 (2025): 104850, https://doi.org/10.1016/j.addma.2025.104850.

64. C. A. Garrido, D. S. Garske, M. Thiele, et al., "Hydrogels with Stiffness-Degradation Spatial Patterns Control Anisotropic 3D Cell Response," *Biomaterials Advances* 151 (2023): 213423, https://doi.org/10.1016/j.bioadv.2023.213423.

65. X.-H. Qin, X. Wang, M. Rottmar, B. J. Nelson, and K. Maniura-Weber, "Near-Infrared Light-Sensitive Polyvinyl Alcohol Hydrogel Photoresist for Spatiotemporal Control of Cell-Instructive 3D Microenvironments," *Advanced Materials* 30, no. 10 (2018): 1705564, https://doi.org/10.1002/adma.201705564.

66. S. Sayer, T. Zandrini, M. Markovic, et al., "Guiding Cell Migration in 3D with High-Resolution Photografting," *Scientific Reports* 12, no. 1 (2022): 8626, https://doi.org/10.1038/s41598-022-11612-y.

67. L. D. D'Andrea, G. Iaccarino, R. Fattorusso, et al., "Targeting Angiogenesis: Structural Characterization and Biological Properties of a De Novo Engineered VEGF Mimicking Peptide," *PNAS* 102, no. 40 (2005): 14215–14220, https://doi.org/10.1073/pnas.0505047102.

68. G. Santulli, M. Ciccarelli, G. Palumbo, et al., "In Vivo Properties of the Proangiogenic Peptide QK," *Journal of Translational Medicine* 7 (2009): 1–10, https://doi.org/10.1186/1479-5876-7-41.

69. B. P. Hung, T. Gonzalez-Fernandez, J. B. Lin, et al., "Multi-Peptide Presentation and Hydrogel Mechanics Jointly Enhance Therapeutic Duo-Potential of Entrapped Stromal Cells," *Biomaterials* 2020 (2019): 119973, https://doi.org/10.1016/j.biomaterials.2020.119973.

70. J. Jia, E. Je Jeon, M. Li, et al., "Evolutionarily Conserved Sequence Motif Analysis Guides Development of Chemically Defined Hydrogels for Therapeutic Vascularization," *Science Advances* 6, no. 28 (2020): 1–16, https://doi.org/10.1126/sciadv.aaz5894.

71. F. González-Pérez, A. Ibáñez-Fonseca, M. Alonso, and J. C. Rodríguez-Cabello, "Combining Tunable Proteolytic Sequences and a VEGF-Mimetic Peptide for the Spatiotemporal Control of Angiogenesis within Elastin-Like Recombinamer Scaffolds," *Acta Biomaterialia* 130 (2021): 149–160, https://doi.org/10.1016/j.actbio.2021.06.005.

72. O. J. Abilez, H. Yang, Y. Guan, et al., "Gastruloids Enable Modeling of the Earliest Stages of Human Cardiac and Hepatic Vascularization," *Science* 388 (2025): adu9375, https://doi.org/10.1126/science.adu9375.

73. P. N. Nwokoye and O. J. Abilez, "Bioengineering Methods for Vascularizing Organoids," *Cell Reports Methods* 4, no. 6 (2024): 100779, https://doi.org/10.1016/j.crmeth.2024.100779.

74. D. J. Carvalho, A. M. Kip, A. Tegel, et al., "A Modular Microfluidic Organoid Platform Using LEGO-like Bricks," *Advanced Healthcare Materials* 13, no. 13 (2024): 2303444, https://doi.org/10.1002/adhm.202303444.

75. E. A. Bulanova, E. V. Koudan, J. Degosserie, et al., "Bioprinting of a Functional Vascularized Mouse Thyroid Gland Construct," *Biofabrication* 9, no. 3 (2017): 034105, https://doi.org/10.1088/1758-5090/aa7fdd.

76. S. Das, W. J. Gordián-Vélez, H. C. Ledebur, et al., "Innervation: the Missing Link for Biofabricated Tissues and Organs," *Npj Regenerative Medicine* 5, no. 1 (2020): 11, https://doi.org/10.1038/s41536-020-0096-1.

77. A. Malheiro, A. Harichandan, J. Bernardi, et al., "3D culture Platform of human iPSCs-derived Nociceptors for Peripheral Nerve Modeling and Tissue Innervation," *Biofabrication* 14, no. 1 (2021): 014105, https://doi.org/10.1088/1758-5090/ac36bf.

Supporting Information

Additional supporting information can be found online in the Supporting Information section.

Supporting file: adhm70575-sup-0001-SuppMat.docx